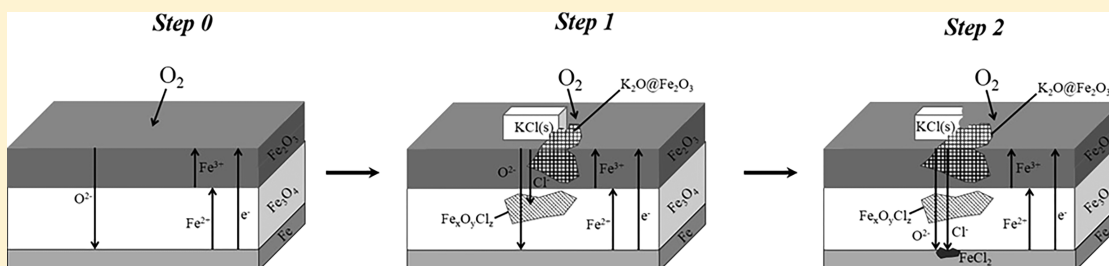


Oxidation Driven Permeation of Iron Oxide Scales by Chloride from Experiment Guided First-Principles Modeling

Valentina Cantatore,*¹ Mercedes Andrea Olivas Ogaz, Jesper Liske,¹ Torbjörn Jonsson, Jan-Erik Svensson, Lars-Gunnar Johansson, and Itai Panas

Environmental Inorganic Chemistry, Department of Chemistry and Chemical Engineering, Chalmers University of Technology, SE-41296 Göteborg, Sweden



ABSTRACT: In this comprehensive investigation, it is demonstrated how chloride ions may permeate a crack-free oxide scale, thus providing hitherto missing mechanistic insight as to the impacts of $KCl(s)$ or $HCl(g)$ exposures on the high-temperature corrosion of biomass- and waste-fired boilers. Guided by dedicated experimental analyses, mechanistic understanding is gained by means of density functional theory. Chloride ions, being accommodated in oxygen anion vacancies that are generated at the receding magnetite/alloy interface, are driven through the oxide scale by the oxidation process. Intermediate stabilities of quasi-homogeneous transient iron oxychloride species are found, employing potassium ferrite and goethite as complementary cation sinks for the $KCl(s)$ and $HCl(g)$ reactants. Spontaneous disproportionation of the supersaturated oxychlorides into two different types of chloride decorated magnetite grain boundaries is demonstrated. These motifs are proposed to explain loss of scale integrity as well as accelerated oxidation by offering short-circuiting transient pathways for ion diffusion.

1. INTRODUCTION

Global warming is a strong driver for developing new technologies for CO_2 -neutral power generation, including the use of biomass and municipal waste as fuels in boilers to generate power as well as heat. Such boilers are known to experience more severe fireside corrosion than plants firing coal or natural gas. In order to mitigate the corrosion of heat transfer surfaces in the waterwalls and in the steam superheater, boilers burning biomass or waste are designed for relatively low steam data and tend to use more expensive, corrosion-resistant alloys. Thus, knowing the mechanisms of corrosion and understanding why the boiler environment is so corrosive will help to solve these operative issues. The relatively high corrosivity in biomass-fired boilers has been attributed to the low sulfur/chlorine ratios and high alkali content^{1–6} of the burned material. Moreover, the even greater corrosivity in waste-fired boilers has been attributed mainly to the high chlorine levels, including both alkali chlorides and $HCl(g)$.^{7–11}

Low alloy steels are preferred materials of construction for heat transfer surfaces in boilers because they combine low cost, good weldability, and excellent mechanical properties. They form Fe_2O_3/Fe_3O_4 oxide scales that provide protection in mildly corrosive environments at <500 °C.¹² To cope with higher temperatures and more corrosive environments, alloys containing >9% chromium are used.^{13–15} Depending on the severity of corrosion, ferritic $FeCr$ steels, austenitic $FeCrNi$ steels, and

austenitic high alloy steels are used. Several studies show that alkali chlorides accelerate the fireside corrosion of all these alloys,^{13–20} resulting in the formation of a porous and layered, poorly protective iron oxide scale with transition metal chlorides in the subscale region. This corrosion type, termed “active oxidation”, has commonly been attributed to a so-called “chlorine cycle”, and several related scenarios are presented in the literature.^{17–22} Shortly, these schemes claim that the corrosiveness of alkali chlorides and HCl toward high temperature steels in the presence of O_2 and H_2O is due to a cyclic process where molecular chlorine plays a catalytic role. In the framework of the “chlorine cycle”, $Cl_2(g)$ is supposed to be generated at the scale surface by oxidation of alkali chlorides or HCl by O_2 . Gaseous chlorine then penetrates to the metal/oxide interface, via cracks and pores in the oxide scale, and reacts with the alloy to form transition metal chlorides (e.g., $FeCl_2$).¹⁷ $FeCl_2$, which is stable in the low oxygen activity conditions presumably prevailing beneath the scale, is then transported in gaseous form to the scale surface where the high pO_2 causes it to decompose spontaneously, forming porous iron oxide. The decomposition is supposed to regenerate Cl_2 which enters the scale again, closing the “chlorine cycle”.¹⁷

Received: July 9, 2019

Revised: September 17, 2019

Published: October 7, 2019

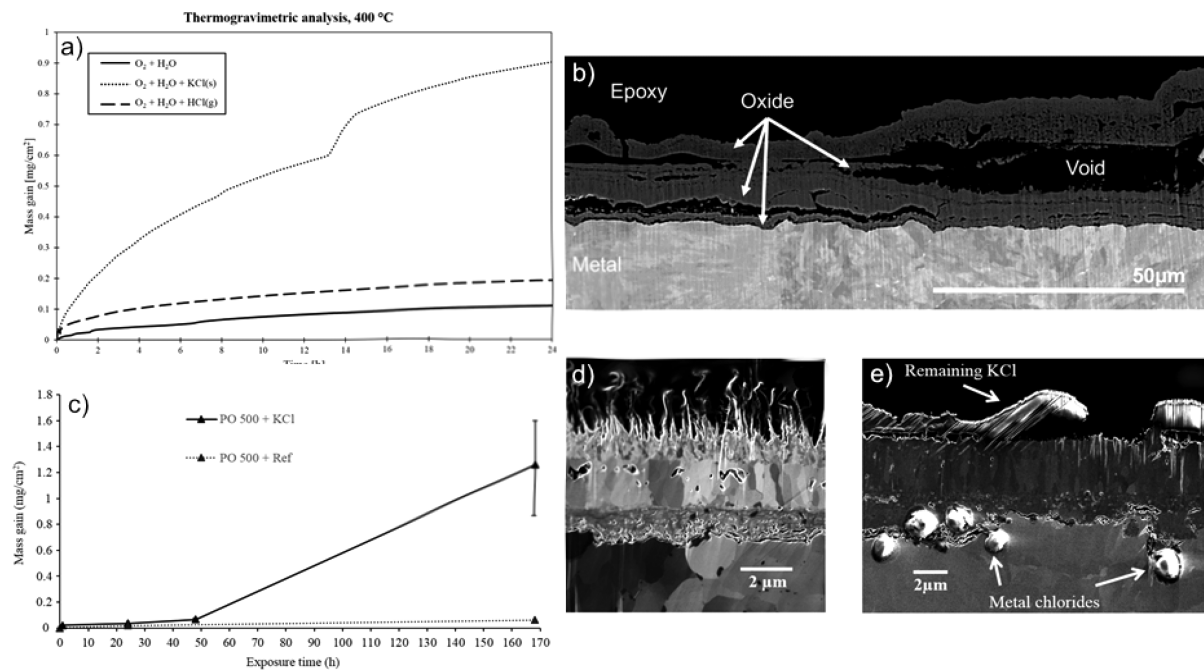
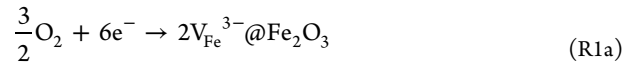


Figure 1. (a) Mass change as a function of time for low alloy steel Fe–2.25Cr–1Mo at 400 °C in N₂ containing 5% O₂ and 20% H₂O: fast O₂ + H₂O + KCl (dotted line), slow O₂ + H₂O (solid line), and intermediate O₂ + H₂O + HCl (dashed line), from ref 16. (b) BSE image of BIB cross section of a Fe–2.25Cr–1Mo exposed at 400 °C for 168 h in N₂ containing 5% O₂ and 40% H₂O; tilted 45°.²⁴ (c) Preoxidation introduced incubation time prior to an accelerated corrosion induced mass gain reported after 1, 24, 48, and 168 h exposure²⁸ at 400 °C in N₂ containing 5% O₂ and 20% H₂O and 0.1 mg/cm² KCl (PO 500 + KCl, solid line) and in the absence of KCl (PO 500 + Ref, dashed line). (d) SE image of BIB cross section after the 12 h preoxidation step. (e) SE image of BIB cross section after 168 h exposure with 0.1 mg/cm² of KCl (cf. (c), solid line). Metal chloride is observed at the alloy/oxide interface in the absence of visible cracks in the oxide scale.

It has been pointed out, however, that the “active oxidation” scenario has several shortcomings.^{13,23,24} For example, it appears unlikely that the highly oxidizing and reactive Cl₂ molecule can penetrate the iron oxide scale and reach the metal substrate without being reduced along the way. Moreover, if cracks are present in the oxide scale through which gaseous Cl₂ can diffuse to the metal/scale interface, the same diffusion paths must also be available for gaseous O₂. The appearance of a crack would indeed disable any possibilities to maintain the oxygen activity gradient across the scale, which is crucial for the “chloride cycle”. Furthermore, the concentration of Cl₂ in a typical boiler environment is expected to be quite small (parts per million ranges), whereas the oxygen content is high (around 5–10%) and, thus, can hardly explain the rapid chlorination reactions observed in many cases. Finally, given that the metal is covered by a continuous and adherent oxide scale before being exposed to the chlorinating agent, then the “active oxidation” scenario cannot explain how chlorination is initiated.

In this context, Folkeson et al.^{23,24} proposed an alternative scenario for steel chlorination by KCl(s) and HCl(g) in the presence of O₂ where chlorine penetrates the scale by solid state diffusion of chloride ions rather than by gas phase diffusion of Cl₂ molecules. Taking this one step further, here we propose Cl[−] to migrate across the continuous oxide scale, diffusing along the oxygen activity gradient of the inward component of the oxide growth process. Indeed, let the oxide scale growth be subdivided into two electrochemical processes: an outward growing hematite channel and an inward growing magnetite channel. The hematite grows by outward diffusion of Fe³⁺ ions:

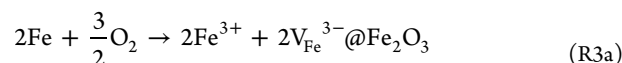
cathode@oxide/gas interface:



anode@alloy/oxide interface:



total:

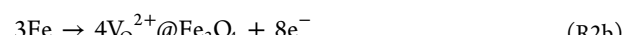


The magnetite grows by inward diffusion of O^{2−} ions:

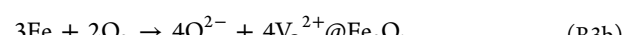
cathode@oxide/gas interface:



anode@alloy/oxide interface:



total:



In reactions R1a–R3a and R1b–R3b, V_xⁿ⁺ indicates the formation of a charged vacancy: V_{Fe}³⁺ in the case of an iron vacancy and V_O²⁺ for an oxygen vacancy. The outward diffusion channel is characterized by cation vacancies implicitly produced by the O₂ reduction that become effectively annihilated by outward diffusion of cations generated at the alloy/oxide interface. Correspondingly, the inward growing magnetite channel is associated with anion vacancies implicitly produced by iron oxidation at the alloy/oxide interface that become annihilated by the inward diffusion of O^{2−} ions. Thus, it is

suggested that chloride may undergo inward diffusion by accessing the anion diffusion channel offered by **reactions R1b–R3b**.

However, while the **reactions R1b–R3b** assisted scheme avoids some inherent problems of the “chlorine cycle” scenario, it also raises new questions. Crucially, it infers that chloride ions diffuse through a continuous oxide scale, while experimental evidence of transient chloride *within* such a scale is lacking.

In what follows, we use theory to further investigate and test the viability of this alternative corrosion scenario^{23,24} which proposes that the transport of chlorine across the scale occurs in the solid state. In particular, density functional theory (DFT) is used to elucidate the electrochemical mechanism for steel chlorination by KCl(s) or HCl(g) in the presence of O₂ and to investigate the energy landscape associated with the process. We show that iron chlorination involving formation of FeCl₂ at the scale/metal interface and KFeO₂ or FeOOH at the top of the scale is spontaneous. We also show that intercalation of iron(II) chloride into magnetite, driven by iron oxidation, is energetically favored, implying easy transport of chloride through magnetite bulk, be it lattice or grain boundaries. The new understanding is used to interpret selected experimental observations concerning the chlorination of steel by KCl(s), and the role of HCl(g).

2. MODELING CONSIDERATIONS

The unraveling of atomistic mechanisms for complex processes such as “active oxidation” relies on experimental model studies to guide the first-principles modeling in order to narrow down the number of a priori possible candidate mechanisms. In the present section, the morphological properties of the growing oxide taken as a point of departure of the present study are described in conjunction with the computational approach. Moreover, validation of the computational scheme for the problem at hand is provided by comparing experimental data to the results from density functional theory calculations.

2.1. Considerations from Experiment. High temperature oxidation of iron in the presence of O₂(g) at <573 °C is reported to result in formation of a continuous and adherent oxide scale consisting of a hematite upper part and a subjacent magnetite part, with the latter in turn consisting of an outer outward growing layer and a bottom, inward growing layer.²⁵ The oxidation behavior of low alloy steels (containing about 2% Cr) in the presence of O₂(g) at <573 °C is similar to that of iron, including the scale growth rate and the scale morphology, with the main difference being that the magnetite in the bottom inward growing part of the scale is replaced by iron–chromium spinel oxide (Fe_{3-x}Cr_xO₄; x < 0.3).²⁶

As presented in the **Introduction**, alkali chlorides and HCl accelerate the corrosion of iron and low alloy steel^{24,27,28} (see **Figure 1a**). Crucially, KCl(s) addition is reported to result in a marked acceleration of scale growth and in a drastic change in the scale morphology, with traces of FeCl₂ appearing at the alloy/scale interface.^{17,18,24,29} The presence of HCl(g) in O₂ + H₂O environment causes less acceleration of scale growth than KCl(s).²⁷ The resulting oxide scale is porous and is made up of multiple consecutive hematite/magnetite (Fe) or hematite/magnetite/FeCr spinel layers (low alloy steel); see **Figure 1b**.

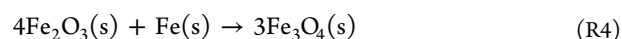
The influence of oxide microstructure on chlorine-induced corrosion has been investigated experimentally²⁸ with a two-step exposure, comprising preoxidation prior to chloride exposure (see **Figure 1c–e**). Chlorine was found to penetrate the dense preformed oxide although no cracks were observed in the oxide before or after the exposure to KCl(s). Correspondingly, the

released potassium must form a compound more stable than KOH(s,l) for chlorination of iron by KCl(s) to be spontaneous.²⁹ This requirement is fulfilled, however, by potassium ferrate(III), KFeO₂(s). Inasmuch as steel chlorination by KCl(s) does produce enrichment of potassium on the outer hematite scale as required, with the concentration of K⁺ reaching about 1 atom %, KFeO₂ was not observed.^{16,27} Yet, the relevance of potassium ferrate(III) is supported by experiments when steel is exposed to K₂CO₃(s) in air at 600 °C.²⁹ Here, KFeO₂ is employed as a potassium sink model as it offers a handy lower bound to the stability of the real potassium sink.

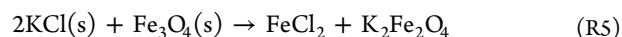
2.2. Computational Details and Methodology. The CASTEP program package within the Material Studios framework¹⁹ was utilized, and the PBE GGA functional³⁰ was employed for all the spin-polarized calculations. Core electrons were described by on-the-fly ultrasoft pseudopotentials³¹ with 571.4 eV cutoff energy together with Koelling–Harmon treatment³² for relativistic effects. The *k*-point sampling of the Brillouin zone was made by means of the Monkhorst–Pack scheme^{33,34} with a 4 × 4 × 4 *k*-point mesh. All the structures were fully optimized using the BFGS algorithm³⁵ with the following set of convergence thresholds: 10⁻⁵ eV/atom for the energy, 0.03 eV/Å for the maximum force, 0.05 GPa for the maximum stress, and 0.001 Å for the maximum displacement. Only neutral unit cells were considered. Indeed, local charge neutrality is an essential element of the emerging understanding. It was ensured by the redox property of the iron ions in that for every O²⁻ that is replaced by Cl⁻ an Fe³⁺ is replaced by an Fe²⁺. The limiting case of this titration process comprises conversion of Fe₃O₄ ⇌ FeO·Fe₂O₃ all the way into Fe₃O₂Cl₂ ⇌ (FeO)₂·FeCl₂. Three model systems were considered: Quasi-homogeneous transient oxychloride structures were derived from the primitive unit cell of the inverse spinel structure Fe₆O₈ of magnetite and supercells addressing segregation of chlorides into layered structures (mono- and bilayered) employing 56 atoms per supercell. The two chloride decorated grain boundary models comprise single-layer “Cl–Fe–O” and double-layer “Cl–Fe–Cl” internal interfaces oriented normal to the 100 direction in the magnetite structure; see below.

2.3. Validation of the Methodology. The ferrimagnetic spin order in the magnetite structure was manually defined by introducing the correct Fe²⁺, Fe³⁺ distribution in the octahedral and tetrahedral sites together with the correct up/down spin orientation³⁶ which is fundamental to obtaining reliable energies and geometrical parameters. To validate the DFT energies obtained for magnetite and for the other species considered in this study, we compared the calculated enthalpies with the corresponding experimental values for key reactions. We have chosen to represent potassium(III) ferrate as K₂Fe₂O₄ rather than as KFeO₂ to simplify and enhance readability. The reaction enthalpies are presented in terms of electronvolts (eV), with 1 eV = 96.4 kJ mol⁻¹.

We start with the reaction that employs hematite to oxidize iron and form magnetite:



This reaction is slightly exothermic with an experimental enthalpy $\Delta H_{\text{exp}} = -0.63$ eV, to be compared with the computed $\Delta H_{\text{DFT}} = -0.93$ eV. Next, we consider the reaction



$$\Delta H_{\text{exp}} = +2.82 \text{ eV}$$

Table 1. Cell Parameters for the Reference Systems^a

system	experiment			unit cell parameters (Å)			%Err		
	<i>a</i>	<i>b</i>	<i>c</i>	<i>a</i>	<i>b</i>	<i>c</i>	<i>a</i>	<i>b</i>	<i>c</i>
FeCl ₂	3.58	3.58	17.54	3.49	3.49	(18.3)	-2.51	-2.51	(4.33)
KCl	6.29	6.29	6.29	6.38	6.38	6.38	1.45	1.45	1.45
K ₂ Fe ₂ O ₄	5.58	11.23	15.89	5.72	11.28	16.15	2.55	0.00	1.61
Fe ₂ O ₃	5.03	5.03	13.75	5.01	5.01	13.90	-0.46	-0.46	1.06
Fe ₃ O ₄	8.39	8.39	8.39	8.41	8.41	8.41	0.13	0.13	0.13
Fe	2.87	2.87	2.87	2.84	2.84	2.84	-1.04	-1.04	-1.04

^aExperimental and DFT values are presented. The percentage of error is calculated according to the formula %Err = $\frac{X_{\text{DFT}} - X_{\text{exp}}}{X_{\text{exp}}} \cdot 100\%$.

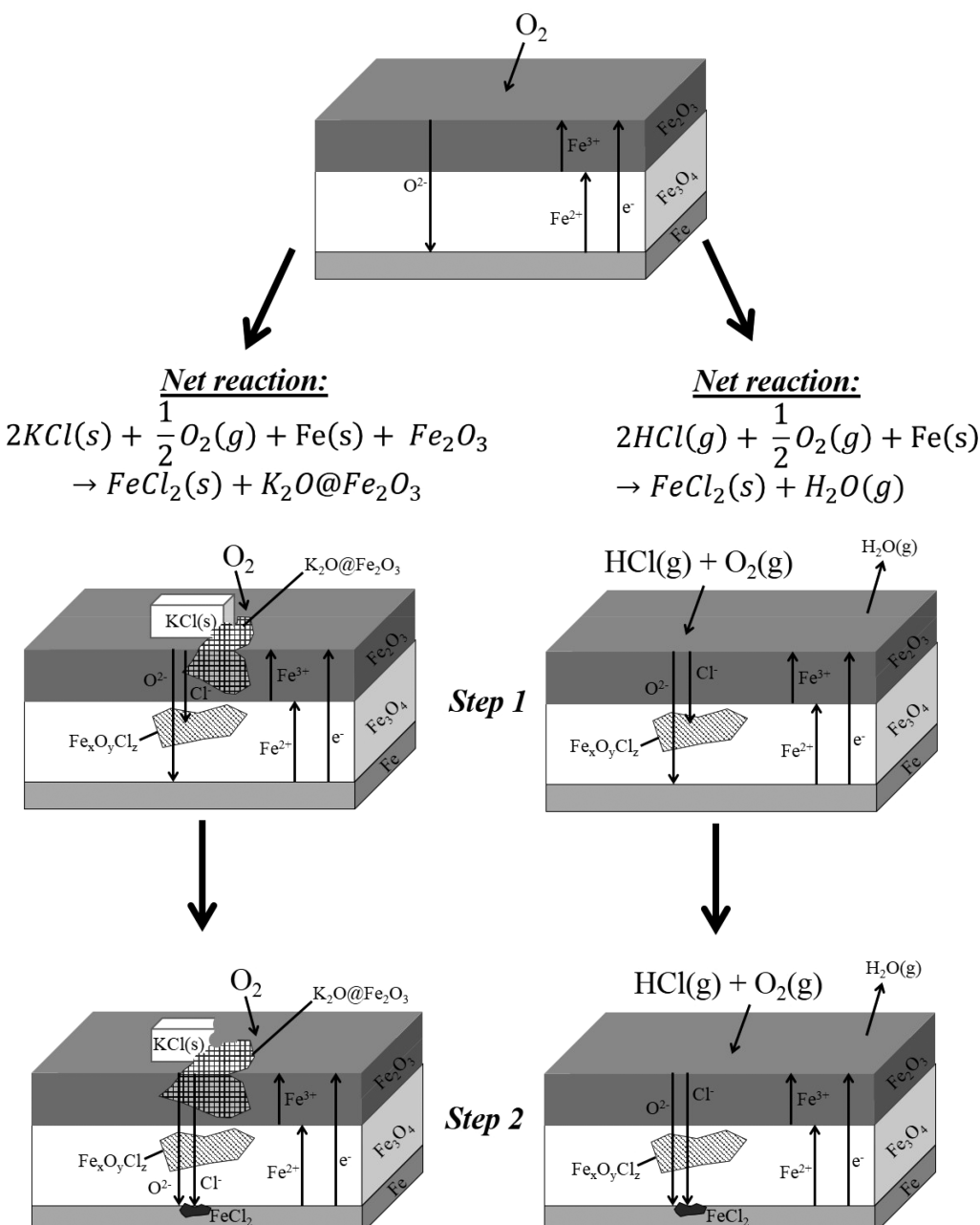


Figure 2. Schematic representation of the corrosion mechanism presented in this article. Hematite, the top oxide (dark gray), is highly porous and thus transparent to KCl. The inner oxide (white) is dense magnetite. The bottom layer (light gray) is the alloy.

$$\Delta H_{\text{DFT}} = +2.95 \text{ eV}$$

We combine reactions R4 and R5 to obtain

Table 2. Energetics for Incorporation of Chlorides of $\text{KCl}(\text{s})$ or $\text{HCl}(\text{g})$ Origins in Magnetite and Subsequent Decomposition of the Resulting Iron Oxychlorides in Reactions with Hematite or Magnetite, To Arrive at $\text{FeCl}_2(\text{s})$ ^a

reaction	ΔH_{DFT} (eV)
Chloride Charging	
$\text{KCl}(\text{s}) + [\text{O}_\text{O}^\text{x}@{\text{magnetite}}] + \text{Fe}(\text{s}) + \frac{1}{2}\text{O}_2(\text{g})$	-0.48
$\rightarrow [\text{Cl}_\text{O}^\text{x}@{\text{magnetite}}] + \frac{1}{2}\text{K}_2\text{Fe}_2\text{O}_4(\text{s})$	
$\text{HCl}(\text{g}) + [\text{O}_\text{O}^\text{x}@{\text{magnetite}}] + \text{Fe}(\text{s}) + \frac{1}{2}\text{O}_2(\text{g})$	-2.94
$\rightarrow [\text{Cl}_\text{O}^\text{x}@{\text{magnetite}}] + \text{FeOOH}(\text{s})$	
decomposition in reaction with hematite	
$[\text{Cl}_\text{O}^\text{x}@{\text{magnetite}}] + \text{Fe}_2\text{O}_3(\text{s})$	-1.17
$\rightarrow [\text{O}_\text{O}^\text{x}@{\text{magnetite}}] + \frac{1}{2}\text{FeCl}_2(\text{s}) + \frac{1}{2}\text{Fe}_3\text{O}_4(\text{s})$	
decomposition in reaction with magnetite	
$[\text{Cl}_\text{O}^\text{x}@{\text{magnetite}}] + \frac{1}{4}\text{Fe}_3\text{O}_4(\text{s}) \rightarrow [\text{O}_\text{O}^\text{x}@{\text{magnetite}}] + \frac{1}{2}\text{FeCl}_2(\text{s}) + \frac{1}{4}\text{Fe}(\text{s})$	-0.96
Chloride Charging	
$\text{KCl}(\text{s}) + [\text{Cl}_\text{O}^\text{x}\text{O}_\text{O}^\text{x}@{\text{magnetite}}] + \text{Fe}(\text{s}) + \frac{1}{2}\text{O}_2(\text{g})$	-0.90
$\rightarrow [\text{Cl}_\text{O}^\text{x}\text{Cl}_\text{O}^\text{x}@{\text{magnetite}}] + \frac{1}{2}\text{K}_2\text{Fe}_2\text{O}_4(\text{s})$	
$\text{HCl}(\text{g}) + [\text{Cl}_\text{O}^\text{x}\text{O}_\text{O}^\text{x}@{\text{magnetite}}] + \text{Fe}(\text{s}) + \frac{1}{2}\text{O}_2(\text{g})$	-3.34
$\rightarrow [\text{Cl}_\text{O}^\text{x}\text{Cl}_\text{O}^\text{x}@{\text{magnetite}}] + \text{FeOOH}(\text{s})$	
decomposition in reaction with hematite	
$[\text{Cl}_\text{O}^\text{x}\text{Cl}_\text{O}^\text{x}@{\text{magnetite}}] + 2\text{Fe}_2\text{O}_3(\text{s})$	-2.02
$\rightarrow [\text{O}_\text{O}^\text{x}\text{O}_\text{O}^\text{x}@{\text{magnetite}}] + \text{FeCl}_2(\text{s}) + \text{Fe}_3\text{O}_4(\text{s})$	
decomposition in reaction with magnetite	
$[\text{Cl}_\text{O}^\text{x}\text{Cl}_\text{O}^\text{x}@{\text{magnetite}}] + \frac{1}{2}\text{Fe}_3\text{O}_4(\text{s})$	-1.55
$\rightarrow [\text{O}_\text{O}^\text{x}\text{O}_\text{O}^\text{x}@{\text{magnetite}}] + \text{FeCl}_2(\text{s}) + \frac{1}{2}\text{Fe}(\text{s})$	
Chloride Charging	
$2\text{KCl}(\text{s}) + [\text{Cl}_\text{O}^\text{x}\text{O}_\text{O}^\text{x}\text{Cl}_\text{O}^\text{x}\text{O}_\text{O}^\text{x}@{\text{magnetite}}] + 2\text{Fe}(\text{s}) + \text{O}_2(\text{g})$	-1.32
$\rightarrow [\text{Cl}_\text{O}^\text{x}\text{Cl}_\text{O}^\text{x}\text{Cl}_\text{O}^\text{x}\text{Cl}_\text{O}^\text{x}@{\text{magnetite}}] + \text{K}_2\text{Fe}_2\text{O}_4(\text{s})$	
$2\text{HCl}(\text{g}) + [\text{Cl}_\text{O}^\text{x}\text{O}_\text{O}^\text{x}\text{Cl}_\text{O}^\text{x}\text{O}_\text{O}^\text{x}@{\text{magnetite}}] + 2\text{Fe}(\text{s}) + \text{O}_2(\text{g})$	-3.36
$\rightarrow [\text{Cl}_\text{O}^\text{x}\text{Cl}_\text{O}^\text{x}\text{Cl}_\text{O}^\text{x}\text{Cl}_\text{O}^\text{x}@{\text{magnetite}}] + \text{FeOOH}(\text{s})$	
decomposition in reaction with hematite	
$[\text{Cl}_\text{O}^\text{x}\text{Cl}_\text{O}^\text{x}\text{Cl}_\text{O}^\text{x}\text{Cl}_\text{O}^\text{x}@{\text{magnetite}}] + 4\text{Fe}_2\text{O}_3(\text{s})$	-4.03
$\rightarrow [\text{O}_\text{O}^\text{x}\text{O}_\text{O}^\text{x}\text{O}_\text{O}^\text{x}\text{O}_\text{O}^\text{x}@{\text{magnetite}}] + 2\text{FeCl}_2(\text{s}) + 2\text{Fe}_3\text{O}_4(\text{s})$	
decomposition in reaction with magnetite	
$[\text{Cl}_\text{O}^\text{x}\text{Cl}_\text{O}^\text{x}\text{Cl}_\text{O}^\text{x}\text{Cl}_\text{O}^\text{x}@{\text{magnetite}}] + \text{Fe}_3\text{O}_4(\text{s})$	-3.11
$\rightarrow [\text{O}_\text{O}^\text{x}\text{O}_\text{O}^\text{x}\text{O}_\text{O}^\text{x}\text{O}_\text{O}^\text{x}@{\text{magnetite}}] + 2\text{FeCl}_2(\text{s}) + \text{Fe}(\text{s})$	

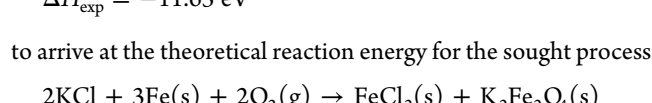
^aThe fate of potassium from $\text{KCl}(\text{s})$ is to form potassium ferrite, while hydrogen from $\text{HCl}(\text{g})$ ends up as the transient iron(III) oxyhydroxide (goethite); cf. **Introduction**.



$$\Delta H_{\text{exp}} = +7.83 \text{ eV}$$

$$\Delta H_{\text{DFT}} = +7.93 \text{ eV}$$

We then employ the experimental energies obtained for the reaction



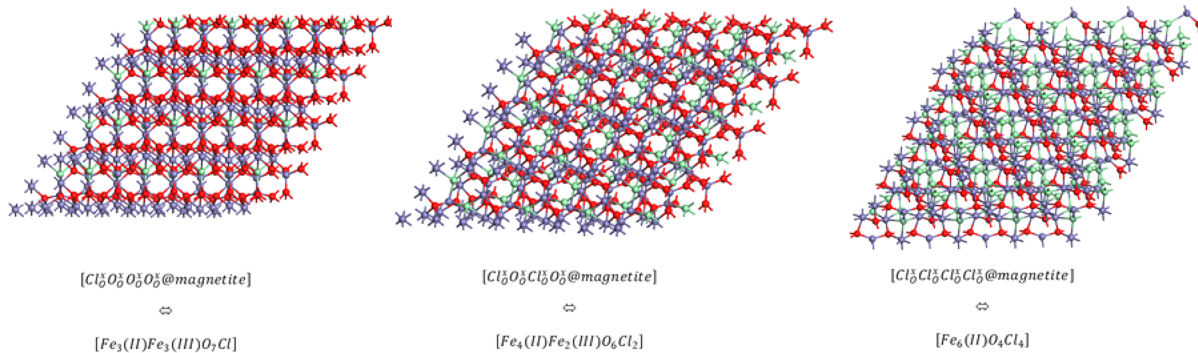


Figure 3. Optimized structures for chloride which is quasi-homogeneously distributed in magnetite, 7.1 atom % Cl (left), 14.2 atom % Cl (center), and 28.4 atom % Cl (right). Modular representations and their compositional equivalents are also shown. Color code: red, oxygen; purple, iron; green, chlorine.

$$\Delta H_{\text{DFT}} = -8.68 \text{ eV}$$

showing that it is spontaneous at all relevant temperatures.

Having thus demonstrated that the reaction energies for the reference systems compare favorably to experiment, further trust emerges by comparing experimental and computed lattice parameters; see Table 1. Indeed, inasmuch as the density determines the external potential, the resulting electron densities of the reference systems are taken to approximate the true densities well, i.e., the computed local internal potential energy surfaces (PESs) approximating the experimental ones. Hence, we may conclude that any ambiguity in the ground state electronic structures, e.g., spin ambiguities in $K_2Fe_2O_4$, Fe_2O_3 , and Fe_3O_4 , have little impact on the resulting PESs for the reference systems. The only outstanding exception is found for the quasi-two-dimensional van der Waals system $FeCl_2$. The deviation is owing to the shallow interplane PES, and it is also the reason why the reaction energy is expected to be insensitive to the interplane distance. It is gratifying to note the somewhat fortuitous resulting agreement between experiment and calculated reaction energies—see reactions R6 and R8—in support of these assumptions.

3. RESULTS AND DISCUSSION

3.1. Mechanism of Chlorination of Steel by KCl and HCl. The fate of KCl, deposited on top of an iron oxide scale in the presence of O_2 and H_2O , is modeled. We consider that, in the absence of KCl, the oxide scale is dense, continuous, and adherent and that scale growth occurs according to Wagner,³⁷ i.e., by cathodic reduction of O_2 at the scale/gas interface and anodic oxidation of iron at the metal/scale interface, the two electrode surfaces being connected by ionic (Fe^{2+} and O^{2-}) and electronic currents. Our working hypothesis is that chloride acts as an oxygen anion equivalent in the growing iron oxide scale. We thus assume that chloride ions reside in oxygen vacancy (V_O) sites and that they acquire mobility owing to the activity gradient in V_O sites (see Figure 2). Because the V_O sites are generated at the alloy/oxide interface, this is also where the chloride ions eventually accumulate, as $FeCl_2$. We thus investigate the possible transport of chloride, originating from both HCl(g) and KCl(s), through the oxygen sublattice in magnetite as well as the role of K^+ in the overall chlorination process.

Having established the viability of the energetics of the key reactions—the conversion of KCl, iron, and iron oxide upon oxidation into new oxide, iron(II) chloride, and transient potassium ions—by comparing DFT first-principles electronic

structure calculations with experiment (see Computational Details and Methodology), the internal consistency of this working hypothesis is tested in two steps. First, the possible existence of oxychloride transients in a magnetite host crystal is validated. Second, the crucial fate of potassium is highlighted. In this case the calculations use potassium(III) ferrate, $K_2Fe_2O_4$, to represent the potassium-enriched hematite observed experimentally when steel corrodes in the presence of $KCl(s)$, O_2 , and H_2O .²⁹ This is because no data is available on potassium-enriched hematite. However, according to ref 38, at low K_2O loads, $K_2O@Fe_2O_3(s)$ (K_2O adsorbed on hematite) is energetically favored in comparison to $K_2Fe_2O_4$. The adsorption of K_2O on hematite is formally analogous to water adsorption and involves K^+ and OK^- entities that form bonds to the hematite surface. The relative stability of $K_2O@Fe_2O_3(s)$ implies that, if the processes investigated turn out spontaneously in the calculations, this outcome does not depend on this particular choice of potassium-containing reaction product.

In what follows, we take the permeation of chloride of both $KCl(s)$ and $HCl(g)$ origins to occur in two steps. (i) The first is incorporation of chloride in the magnetite lattice accompanied by the corresponding formation of $K_2Fe_2O_4$ (from $KCl(s)$) and $FeOOH$ (goethite; from $(HCl(g))$) as driven by the oxidation of iron by $O_2(g)$. Here, a quasi-homogeneous substitutional chloride doping is explored and contrasted by the formation of segregated single- and double-layer chlorides in the magnetite structure. (ii) The second step is recovery of the magnetite lattice by reaction with hematite or magnetite (see section 3.2 and Table 2). In the latter case, wüstite (FeO from now on) and $FeCl_2$ are formed, the former being taken to disproportionate into iron and magnetite.

3.2. Possible Quasi-Homogeneous Oxychloride Transients. In this section, we investigate stabilities of possible intermediaries that may support a viable path for chloride permeation through a magnetite scale. For bookkeeping we introduce the nomenclature $[O_O^x @magnetite]$ as lattice oxygen ions to be replaced by chloride ions (see Figure 3). In the present study $[O_O^x @magnetite] \Leftrightarrow [Fe_6O_8]$. We explore the ability of chloride ions to permeate magnetite by considering an initial chloride charging reaction followed by a discharging step. It is noted that because $[Fe_6O_8]$ comprises $[Fe_2(II)Fe_4(III)O_8]$, the intermediate $[Cl_O^x @magnetite]$ comprises $[Fe_3(II)Fe_3(III)O_7Cl]$, i.e., corresponding to an effective reduction of magnetite which is compensated for by the oxidation of Fe. It is noted that this reduction may continue until all $Fe(III)$ is converted into $Fe(II)$, i.e., 50% of the oxygen ions in magnetite being replaced

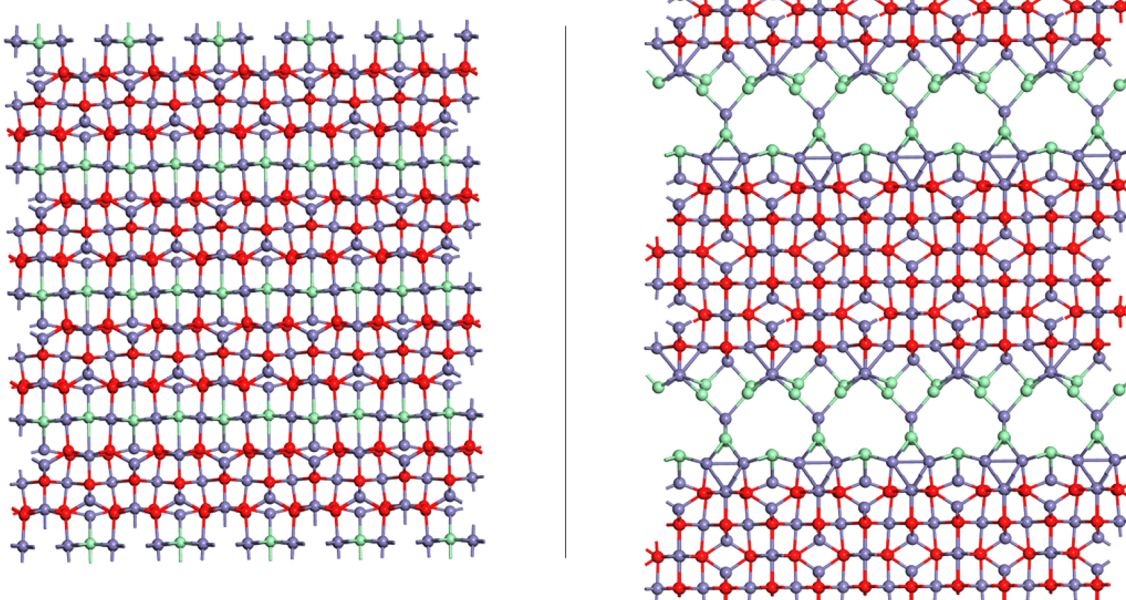
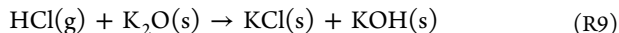


Figure 4. Layered distribution of Cl in magnetite. The number of Cl atoms in the supercell corresponds to 14.3 atom %. Left, monolayer; right, bilayer. Color code: red, oxygen; purple, iron; green, chlorine.

by chloride ions. Besides the incorporation of chloride ions into magnetite, the net chloride charging reaction involves the disposal of potassium as potassium ferrite $K_2Fe_2O_4(s)$ if the source of chloride is $KCl(s)$, and as $FeOOH$ (goethite) if the source is $HCl(g)$. Inasmuch as exclusively solid-state reactions are resorted to in the present study, the total energy of $HCl(g)$ is obtained from the experimental reaction enthalpy $\Delta H_{(Exp)}$ for



This $\Delta H_{(Exp)}$ is also arrived at by subtracting computed total energies of reactants from computed total energies of products:

$$\begin{aligned} \Delta H_{(Exp)} = & E[KCl(s)] + E[KOH(s)] - E[HCl(g)] \\ & - E[K_2O(s)] \end{aligned} \quad (E1)$$

Since $E[KCl(s)]$, $E[OH(s)]$, and $E[K_2O(s)]$ are all computed by DFT in the present study and $\Delta H_{(Exp)}$ of reaction R9 is known, it follows that the unknown $E[HCl(g)]$ may be extracted from eq E1. This procedure is validated for

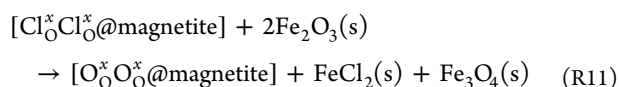


$$\Delta H_{(Exp)} = -1.51 \text{ eV}$$

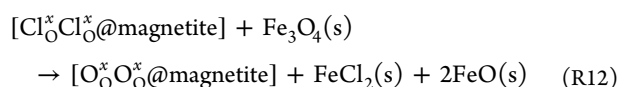
$$\Delta H_{(DFT)} = -1.25 \text{ eV}$$

This is deemed acceptable since the accuracy is similar to what is found for the corresponding reaction with $KCl(s)$ as chloride source; cf. reaction R5.

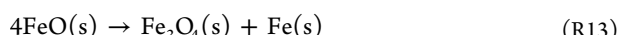
Table 2 quantifies the energetics of emerging viable paths for chloride permeation through crack-free magnetite, comprising charging, enrichment, and decomposition of transient oxychlorides. Said decomposition may involve either hematite or magnetite as reactants. In the case hematite, $FeCl_2$ and magnetite are produced, e.g.



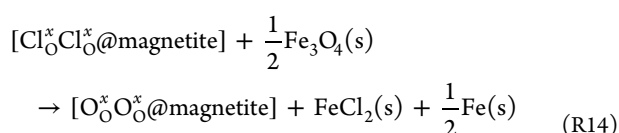
In the case of magnetite as reactant, $FeCl_2$ and Fe are arrived at in two steps, e.g.



followed by



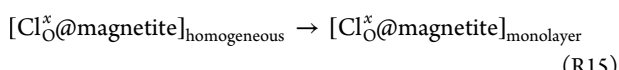
effectively resulting in



Indeed, support for a working hypothesis that allows enrichment of transient oxychloride up to 28 atom %, as driven by the oxidation process, is provided.

3.3. Possible Segregation of Oxychloride in the Oxide Scale. It is emphasized that the proposed mechanism for chloride permeation is driven by metal oxidation, allowing an effectively supersaturated iron oxychloride system to be maintained at steady state. It is noted that the decomposition of this metastable state will result in formation of a mixture of magnetite and iron chloride. It becomes interesting to trace the origin of that reaction by exploring any tendency toward local disproportionation of a quasi-homogeneous distribution of oxychloride in magnetite.

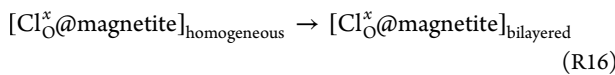
Here, we compare segregations of the quasi-homogeneous oxychloride structures into embedded monolayer and bilayer $FeCl$ motifs (see Figure 4). The enthalpy changes for the transformations come out at



$$\Delta H_{DFT}(7.1 \text{ atom \% Cl}) = -0.23 \text{ eV}$$

$$\Delta H_{\text{DFT}}(14.3 \text{ atom \% Cl}) = 0.50 \text{ eV}$$

and



$$\Delta H_{\text{DFT}}(7.1 \text{ atom \% Cl}) = -0.50 \text{ eV}$$

The monolayered motif is enthalpically favored at low concentrations. At high concentrations, beyond ~ 10 atom % Cl^- , it is destabilized because of buildup of interlayer repulsion. In contrast, the bilayer structure is beneficial at considerably higher concentrations of Cl^- .

3.4. Nonequilibrium Thermodynamics Considerations. Because the quasi-homogeneous transient oxychlorides, formed together with $\text{Fe}(\text{III})\text{OOH}$ and potassium ferrite, display remarkable stabilities, the existence of related extended chloride motifs embedded in magnetite also becomes justified. Here, the stabilities of these transient motifs are taken to support the notion of viable pathways for transport of Cl_O^x through magnetite, tracking the oxygen activity gradient.

While our DFT calculations show that the formation of transient oxychlorides in magnetite is enthalpically favored, and this irrespective of $\text{KCl}(\text{s})$ or $\text{HCl}(\text{g})$ as chloride sources (see Table 2), the decrease in entropy associated with corresponding chloride charging reactions means that the formation of the various oxychloride motifs is only spontaneous up to a certain limiting temperature. Lower bounds to the equilibrium temperature for oxidation-driven chloride permeation are computed for both chloride sources. In the case of $\text{KCl}(\text{s})$, entropy change upon formation of potassium ferrite and iron oxychlorides is restricted to the loss of translational entropy owing to $\text{O}_2(\text{g})$ capture. In the case of $\text{HCl}(\text{g})$, entropy change upon formation of hematite, as $\text{Fe}(\text{III})\text{OOH}$ (goethite) decomposes into hematite and water, and iron oxychlorides includes besides the loss of translational entropy owing to capture of $\text{HCl}(\text{g})$ and $\text{O}_2(\text{g})$ also the entropy gain resulting from H_2O release.

For different chloride concentrations, the maximum temperatures for spontaneous formation of the oxychloride transients, whether monolayered, bilayered, or quasi-homogeneous, are

Table 3. Maximum Temperatures (K) for Spontaneous Formation of the Oxychloride Transients (Embedded in the Magnetite Host), Whether Monolayered, Bilayered, or Quasi-Homogeneous^a

	KCl (K)	KCl (S_{conf}) (K)	HCl (K)	HCl (S_{conf}) (K)
homogeneous (%)				
12.25	608.98	788.17	1803.37	2026.07
25	875.41	1070.34	1926.0	2111.96
50	856.37	968.83	1478.26	1566.17
monolayer (%)				
12.5	900.32		1944.45	
25	241.09		1619.31	
bilayer (%)				
12.5	1243.34		2110.06	
25	1598.58		2275.63	

^aThe impact of configurational entropy is calculated according to eqs E3 and E4.

summarized in Table 3. Given that $\Delta G = 0$ at equilibrium, we may compute the corresponding temperature:

$$T = \Delta H_{\text{DFT}}/\Delta S \quad (\text{E2})$$

For $\text{KCl}(\text{s})$

$$\Delta S_{\text{KCl}} = -\frac{1}{2}S_{\text{O}_2}^{\text{trans}} \quad (\text{E3})$$

while for $\text{HCl}(\text{g})$

$$\Delta S_{\text{HCl}} = \frac{1}{2}S_{\text{H}_2\text{O}}^{\text{trans}} - \frac{1}{2}S_{\text{O}_2}^{\text{trans}} - \frac{1}{2}S_{\text{HCl}}^{\text{trans}} \quad (\text{E4})$$

Thus, it is assumed here that the rotational and vibrational entropy contributions to the reaction entropy change cancel. The additional assumption is to take the configurational entropy change to be negligible. It is justifiable in the cases of chloride ion incorporation in the mono- and bilayered structures. It is however not trivially so in the quasi-homogeneous case where the thermodynamic stability of the transient is indeed underestimated. Correction for the chloride configurational entropy

$$\Delta S^{\text{conf}} = \frac{R}{m} \ln\left(\frac{N!}{m!(N-m)!}\right) \quad (\text{E5})$$

for the transient is arrived at by assuming all oxychloride configurations for a given concentration to display approximately equal enthalpic stabilities. Here, $N = 8$ and $m = 1, 2, 3, 4$. Thus, the quasi-homogeneous oxychlorides extend the range of transient stabilities at experimentally relevant temperatures, particularly in the case of $\text{KCl}(\text{s})$ as chloride source. The relevance of configurational entropy for these kinetic processes may be questioned on the basis of the time scales of the permeation process. Here, we take the entropic impact to rather reflect the manifold of permeation paths for chloride through the magnetite scale. Also, it is noted how the equilibrium stabilities of the oxychlorides of $\text{HCl}(\text{g})$ origin are overwhelmingly favored. This, and the fact that oxidation in the presence of $\text{HCl}(\text{g})$ is much slower than in the presence of $\text{KCl}(\text{s})$, is taken to support a catalytic mechanism for oxidation in the case of the latter.

4. CONCLUDING REMARKS

Any claim of a viable reaction scheme able to describe the “active oxidation” of iron and low alloy steel induced by alkali chlorides or HCl at high temperature should explain *first* the chlorination process per se including chlorine permeation through the scale, and *second* how small amounts of chlorinating agent may have large accelerating effects on the corrosion. Here, a chlorination scenario that satisfies said requirements was offered and validated by first-principles modeling employing density functional theory. While discarding any a priori roles of grain boundaries, essential remaining segments of the energy landscape for chlorine transport across crack-free inner magnetite, including secondary spontaneous a posteriori grain boundary generation, were provided.

4.1. Chlorine Transport across the Oxide Scale, Forming FeCl_2 at the Alloy/Scale Interface. It was shown that the inward growing, magnetite forming oxidation channel is able to accommodate chloride ions; i.e., formation of metastable $\text{Fe}_3\text{O}_{4-x}\text{Cl}_x$ is spontaneous in conjunction with $\text{K}_2\text{Fe}_2\text{O}_4$ or FeOOH , when driven by the oxidation reaction. The latter two compounds are taken to offer transient sinks for K^+ (in the case

of KCl) and H⁺ (in the case of HCl), respectively. These support the claim by offering lower bounds to the corresponding drives for transient chloride incorporation in the magnetite, which in turn spontaneously transforms into FeCl₂, Fe(s), and magnetite. Thus, the diffusion of chloride ions through the inner magnetite scale along the oxygen activity gradient explains the observed accumulation of FeCl₂ at the receding magnetite/alloy interface. It is inferred that chloride ions indeed substitute for O²⁻ ions in the inward transport of anions (outward diffusion of oxygen vacancies V_O²⁺). Hence, viability of chloride diffusion across the magnetite scale by accommodation in oxygen vacancies created by the iron oxidation; i.e., Cl⁻@V_O²⁺, was validated.

4.2. Chlorination Induced Accelerated Loss of Oxide Scale Integrity. It was demonstrated that, as a consequence of the transient supersaturation of chloride in metastable Fe₃O_{4-x}Cl_x spontaneous disproportionation inside the inner magnetite scale is possible. Indeed, two different Cl⁻ decorated magnetite grain boundaries were shown to become accessible. These may in turn offer candidate short-circuiting pathways for both anions and cations through the scale but also render the scale vulnerable to erosion by flaking.

In conclusion, the presented mechanism has avoided several problems associated with the “chlorine cycle” and similar mechanisms by assuming an oxidation assisted permeation mechanism for chloride. It has provided DFT validated accessibility of intermediate oxychloride species that allows chloride ions to be transported across a crack-free magnetite scale and to become enriched as FeCl₂ at the alloy/oxide interface. Moreover, cause for accelerated corrosion was proposed based on DFT validated spontaneous disproportionation of said intermediate oxychlorides into chloride decorated magnetite grain boundaries, supporting rapid oxidation as well as oxide scale degradation. Finally, inasmuch as the inward diffusion of chloride utilizes oxygen vacancies, this anionic pathway does not compete with any outward diffusion of cations such as iron ions.

AUTHOR INFORMATION

Corresponding Author

*E-mail: valcan@chalmers.se.

ORCID

Valentina Cantatore: 0000-0003-2542-5550

Jesper Liske: 0000-0001-8013-3556

Notes

The authors declare no competing financial interest.

ACKNOWLEDGMENTS

This work was carried out at the Swedish High Temperature Corrosion Center (HTC) at Chalmers University of Technology. All the calculations were performed using the resources at the Swedish National Infrastructure for Computing at Chalmers (C3SE).

REFERENCES

- (1) Nielsen, H. P.; Frandsen, F. J.; Dam-Johansen, K.; Baxter, L. L. The implications of chlorine-associated corrosion on the operation of biomass-fired boilers. *Prog. Energy Combust. Sci.* **2000**, *26* (3), 283–298.
- (2) Henderson, P. J.; Karlsson, A.; Davis, C.; Rademakers, P.; Cizner, J.; Formanek, B.; Göransson, K.; Oakley, J. In-situ Fireside Corrosion Testing of Advanced Boiler Materials with Divers Fuels. *Schr. Forschungszent. Juelich, Reihe Energietech./Energy Technol.* **2002**, *21* (2), 785–799.
- (3) Salmoja, K. *Field and Laboratory Studies on Chlorine-Induced Superheater Corrosion in Boilers Fired with Biofuels*; Åbo Akademi: Turku, Finland, 2000.
- (4) Davidsson, K. O.; Åmand, L.-E.; Leckner, B.; Kovacevik, B.; Svane, M.; Hagström, M.; Pettersson, J. B. C.; Pettersson, J.; Asteman, H.; Svensson, J.-E.; Johansson, L.-G. Potassium, Chlorine, and Sulfur in Ash, Particles, Deposits, and Corrosion during Wood Combustion in a Circulating Fluidized-Bed Boiler. *Energy Fuels* **2007**, *21* (1), 71–81.
- (5) Michelsen, H. P.; Frandsen, F.; Dam-Johansen, K.; Larsen, O. H. Deposition and high temperature corrosion in a 10 MW straw fired boiler. *Fuel Process. Technol.* **1998**, *54* (1), 95–108.
- (6) Jenkins, B. M.; Baxter, L. L.; Miles, T. R.; Miles, T. R. Combustion properties of biomass. *Fuel Process. Technol.* **1998**, *54* (1), 17–46.
- (7) Folkeson, N.; Pettersson, J.; Pettersson, C.; Johansson, L. G.; Skog, E.; Andersson, B. A.; Enestam, S.; Tuiremo, J.; Jonasson, A.; Heikne, B.; Svensson, J. E., Fireside corrosion of stainless and low alloyed steels in a waste-fired CFB boiler; The effect of adding sulphur to the fuel. In *High Temperature Corrosion and Protection of Materials 7, Pts 1 and 2*; Steinmetz, P., Wright, I. G., Galerie, A., Monceau, D., Mathieu, S., Eds.; Trans Tech Publications Ltd.: Stäfa, Switzerland, 2008; Vol. 595–598, pp 289–297.
- (8) Karlsson, S.; Pettersson, J.; Åmand, L. E., Reducing high temperature corrosion when burning waste by adding digested sewage sludge. In *Proceedings of The Swedish-Finnish Flame Days*; International Flame Research Foundation: 2011.
- (9) Pettersson, J.; Pettersson, C.; Folkeson, N.; Johansson, L. G.; Skog, E.; Svensson, J. E. The Influence of Sulphur Additions on the Corrosive Environment in a Waste-Fired CFB Boiler. *Mater. Sci. Forum* **2006**, *522–523*, 563–570.
- (10) Kassman, H.; Pettersson, J.; Steenari, B.-M.; Åmand, L.-E. Two strategies to reduce gaseous KCl and chlorine in deposits during biomass combustion — injection of ammonium sulphate and co-combustion with peat. *Fuel Process. Technol.* **2013**, *105*, 170–180.
- (11) Steinmetz, P.; Rapin, C. Corrosion of Metallic Materials in Waste Incinerators. *Mater. Sci. Forum* **1997**, *251–254*, 505–518.
- (12) Kofstad, P. *High Temperature Corrosion*; Elsevier Applied Science: London, 1988.
- (13) Pettersson, J.; Asteman, H.; Svensson, J. E.; Johansson, L. G. KCl induced corrosion of a 304-type austenitic stainless steel at 600 degrees C; The role of potassium. *Oxid. Met.* **2005**, *64* (1–2), 23–41.
- (14) Karlsson, S.; Pettersson, J.; Johansson, L. G.; Svensson, J. E. Alkali Induced High Temperature Corrosion of Stainless Steel: The Influence of NaCl, KCl and CaCl₂. *Oxid. Met.* **2012**, *78* (1–2), 83–102.
- (15) Reese, E.; Grabke, H. J. Einfluß von Natriumchlorid auf die Oxidation von hochlegierten Chrom- und Chrom-Nickel-Stählen. *Mater. Corros.* **1993**, *44* (2), 41–47.
- (16) Persdotter, A.; Sattari, M.; Larsson, E.; Olivas-Ogaz, M. A.; Liske, J.; Jonsson, T. Oxidation of Fe-2.25Cr-1Mo in presence of KCl(s) at 400 °C - crack formation and its influence on oxidation kinetics. *Corros. Sci.* **2019**, DOI: 10.1016/j.corsci.2019.108234.
- (17) Grabke, H. J.; Reese, E.; Spiegel, M. The Effects of Chlorides, Hydrogen-Chloride, and Sulfur-Dioxide in the Oxidation of Steels Below Deposits. *Corros. Sci.* **1995**, *37* (7), 1023–1043.
- (18) Reese, E.; Grabke, H. J. Einfluß von Chloriden auf die Oxidation des 21/4 Cr-1 Mo-Stahls. *Mater. Corros.* **1992**, *43* (12), 547–557.
- (19) Bramhoff, D.; Grabke, H.; Reese, E.; Schmidt, H. Einfluß von HCl und Cl₂ auf die Hochtemperaturkorrosion des 2 1/4 Cr 1 Mo-Stahls in Atmosphären mit hohen Sauerstoffdrücken. *Mater. Corros.* **1990**, *41* (6), 303–307.
- (20) Haanappel, V. A. C.; Haanappel, N. W. J.; Fransen, T.; van Corbach, H. D.; Gellings, P. J. Corrosion Kinetics of Low-Alloy and High-Alloy Steels in Chlorine-Containing Gas Atmospheres. *Corrosion* **1992**, *48* (10), 812–821.
- (21) Lee, Y. Y.; McNallan, M. J. Ignition of nickel in environments containing oxygen and chlorine. *Metall. Mater. Trans. A* **1987**, *18* (6), 1099–1107.
- (22) Abels, J. M.; Strehblow, H. H. A surface analytical approach to the high temperature chlorination behaviour of inconel 600 at 700 °C. *Corros. Sci.* **1997**, *39* (1), 115–132.

- (23) Folkeson, N.; Johansson, L. G.; Svensson, J. E. Initial stages of the HCl-induced high-temperature corrosion of alloy 310. *J. Electrochem. Soc.* **2007**, *154* (9), C515–C521.
- (24) Folkeson, N.; Jonsson, T.; Halvarsson, M.; Johansson, L. G.; Svensson, J. E. The influence of small amounts of KCl(s) on the high temperature corrosion of a Fe-2.25Cr-1Mo steel at 400 and 500 degrees C. *Mater. Corros.* **2011**, *62* (7), 606–615.
- (25) Atkinson, A.; Taylor, R. I.; Hughes, A. E. A quantitative demonstration of the grain boundary diffusion mechanism for the oxidation of metals. *Philos. Mag. A* **1982**, *45* (5), 823–833.
- (26) Pujilaksono, B.; Jonsson, T.; Heidari, H.; Halvarsson, M.; Svensson, J. E.; Johansson, L. G. Oxidation of Binary FeCr Alloys (Fe-2.25Cr, Fe-10Cr, Fe-18Cr and Fe-25Cr) in O₂ and in O₂ + H₂O Environment at 600 degrees C. *Oxid. Met.* **2011**, *75* (3–4), 183–207.
- (27) Larsson, E. *The Corrosive Effect of Chlorine Containing Species on Waterwalls and Superheater Materials in Waste and Biomass-Fired Power Plants*. Ph.D. Thesis, Chalmers University of Technology, Göteborg, 2016.
- (28) Olivas-Ogaz, M. A.; Eklund, J.; Persdotter, A.; Sattari, M.; Liske, J.; Svensson, J.-E.; Jonsson, T. The Influence of Oxide-Scale Microstructure on KCl(s)-Induced Corrosion of Low-Alloyed Steel at 400 °C. *Oxid. Met.* **2019**, *91*, 291.
- (29) Olivas-Ogaz, M. A.; Eklund, J.; Svensson, J.-E.; Liske, J.; Jonsson, T. Microstructural Study of the Influence of KCl and HCl on Preformed Corrosion Product Layers on Stainless Steel. *Oxid. Met.* **2017**, *87* (5), 801–811.
- (30) Perdew, J. P.; Burke, K.; Ernzerhof, M. Generalized Gradient Approximation Made Simple. *Phys. Rev. Lett.* **1996**, *77* (18), 3865–3868.
- (31) Vanderbilt, D. Soft self-consistent pseudopotentials in a generalized eigenvalue formalism. *Phys. Rev. B: Condens. Matter Mater. Phys.* **1990**, *41* (11), 7892–7895.
- (32) Koelling, D. D.; Harmon, B. N. A technique for relativistic spin-polarised calculations. *J. Phys. C: Solid State Phys.* **1977**, *10* (16), 3107–3114.
- (33) Monkhorst, H. J.; Pack, J. D. Special points for Brillouin-zone integrations. *Phys. Rev. B* **1976**, *13* (12), 5188–5192.
- (34) Pack, J. D.; Monkhorst, H. J. "Special points for Brillouin-zone integrations"—a reply. *Phys. Rev. B* **1977**, *16* (4), 1748–1749.
- (35) Pfrommer, B. G.; Côté, M.; Louie, S. G.; Cohen, M. L. Relaxation of Crystals with the Quasi-Newton Method. *J. Comput. Phys.* **1997**, *131* (1), 233–240.
- (36) Martin, G. J.; Cutting, R. S.; Vaughan, D. J.; Warren, M. C. Bulk and key surface structures of hematite, magnetite, and goethite: A density functional theory study. *Am. Mineral.* **2009**, *94* (10), 1341–1350.
- (37) Wagner, C. Beitrag zur Theorie des Anlaufvorgangs. *Z. Phys. Chem.* **1933**, *21B*, 25–41.
- (38) Kotarba, A.; Kruk, I.; Sojka, Z. Energetics of Potassium Loss from Styrene Catalyst Model Components: Reassignment of K Storage and Release Phases. *J. Catal.* **2002**, *211* (1), 265–272.